Acta Cryst. (1993). D**49**, 580–587

A Monoclinic Crystal with *R*32 Pseudo-Symmetry: a Preliminary Report of Nodamura Virus Structure Determination

BY ADAM ZLOTNICK, BONNIE R. MCKINNEY, SANJEEV MUNSHI, JODI BIBLER, MICHAEL G. ROSSMANN AND JOHN E. JOHNSON*

Department of Biological Sciences, Purdue University, West Lafayette, IN 47907, *USA*

(*Received* 5 *January* 1993; *accepted* 12 *July* 1993)

Abstract

We have crystallized Nodamura virus, a $T = 3$ icosahedral virus that can infect both mammalian and insect hosts. Crystals are monoclinic, with two crystallographically independent virus molecules per asymmetric unit. Packing analysis reveals a pseudo-rhombohedral (pseudo-*C*2 in the monoclinic setting) arrangement of virus particles in the crystal lattice. Crystals differ from the *R*32 symmetry by rotational and translational deviations. The rhombohedral packing arrangement and its failure to describe the exact virus packing is analyzed in detail. The icosahedral threefold axis is rotated from the body diagonal of the pseudo-rhombohedral cell, breaking the rhombohedral symmetry. The *C*2 pseudo-symmetry breaks down rotationally and/or translationally.

Introduction

Nodamura virus (NOV) is the type member of the Nodaviridae family (for reviews see Kaesberg, 1987; Hendry, 1991). The usual host of the Nodaviridae is insects; however, NOV can also infect and kill suckling mice. Other vertebrates may be suitable hosts to NOV; swine and herons in NOV's indigenous region in Japan carry antibodies to the virus. The unusually broad host range makes NOV unique among the Nodaviridae and rare among viruses. The Nodaviridae are small $T = 3$ icosahedral viruses (Hosur *et al.*, 1987). Each virion contains both molecules of the bipartite positive-sense RNA genome (Newman & Brown, 1977). The genome codes for only three proteins: protein *A* (an RNA-dependent RNA polymerase factor), protein *B* (unknown function) and protein α (the coat protein) (Newman *et al.*, 1978; Dasgupta & Sgro, 1987). The simplicity of NOV makes it an attractive model system for investigating the propagation, construction and assembly of animal viruses.

* Corresponding author.

The biology and structure of three nodaviruses, NOV, Flock House virus (FHV), and black beetle virus (BBV), have been studied in some detail. Nodaviruses are initially synthesized, *in vivo*, as an immature provirion (Gallagher & Rueckert, 1988). The provirion consists of the genomic RNA and 180 copies of the 43 kDa coat protein, α. The provirion of FHV is not infective (Schneeman, Zhong, Gallagher & Rueckert, 1992) and is much less stable to denaturants than the mature virus (Gallagher & Rueckert, 1988). The provirion matures by autoproteolytic cleavage of α to the N-terminal β protein (363 residues) and the 44-residue γ peptide (Hosur *et al.*, 1987). In FHV and BBV most of α protein cleaves autocatalytically in a matter of a few hours (Gallagher & Rueckert, 1988). A mechanism for this cleavage has recently been proposed (Zlotnick *et al.*, 1993).

Crystal structures are known for BBV (Hosur *et al.*, 1987) and FHV (Fisher, McKinney, Wery & Johnson, 1992). These two viruses, which share >80% identity in their coat protein sequence and concomitantly similar structures of their eight-stranded β-barrel core, show notable differences in the conformation of the inner surface of the virus and the ordering of viral RNA. Ordered RNA at the interface between icosahedral asymmetric units, particularly clear in the FHV electron density map, may have a role in stabilizing the $T = 3$ structure (Fisher & Johnson, 1993). Calcium has a structural role in subunit–subunit interactions within the FHV and BBV asymmetric unit. Gallagher & Rueckert (1988) observed that FHV provirion stability is increased by addition of calcium.

The NOV coat protein has considerable homology with other members of the nodavirus family (Kaesberg *et al.*, 1990), yet it has a notably different host range and physico-chemical properties. NOV is less stable to denaturants and to salt than FHV and BBV. Exposure of NOV to millimolar concentrations of Cl^- is sufficient to reduce infectivity by a log or more (Newman *et al.*, 1978). Similar treatment has no effect on BBV or FHV. We have observed that

Cl^- considerably decreases the stability of NOV (Tucker, 1990; Zlotnick, unpublished results).

NOV has been crystallized in a monoclinic space group with two non-crystallographically related virions per asymmetric unit. The unit-cell space group can be described as slightly distorted *R*32 with one virus per unit cell. In this paper we discuss the *R*32 packing model and show where the actual virus position and orientation deviate from the *R*32 special positions.

Materials and methods

Virus propagation and purification

NOV was grown in wax moth larvae and purified according to the procedure of Selling (1986), briefly summarized here. Wax moth larvae were injected with 5 μl of 5 μg ml^{-1} NOV in 50 m*M* $NaHPO_4$ at pH 7 (phosphate buffer). Two weeks post infection, larvae were removed from their growth medium and frozen at 253 K. In a typical purification, 20 g of frozen larvae were homogenized in 50 ml of cold phosphate buffer. The slurry was centrifuged at 6000 r min^{-1} at 277 K for 15 min to remove cell debris. The pellet was extracted with 50 ml of buffer and again the debris was removed by low-speed centrifugation. The supernatants were pooled, then stirred with 50 ml of chloroform for 20 min at room temperature. The mixture was separated by centrifugation at 2000 r min^{-1} for 15 min at room temperature. The aqueous layer was collected and clarified by centrifugation at 10 000 r min^{-1} for 10 min at 277 K. The virus, in the supernatant, was concentrated by centrifugation through a 30% sucrose cushion in phosphate bufer at 45 000 r min^{-1} for 2 h. The resuspended pellet was banded on a 30 ml 25% sucrose–phosphate buffer freeze–thaw gradient (Davis & Pearson, 1978). The gradient was centrifuged at 25 000 r min^{-1} in a Beckman SW28 rotor at 277 K. The opalescent bands were pooled and concentrated by centrifugation at 45 000 r min^{-1} for 2 h. The pellet was resuspended in phosphate buffer. A typical yield was 10–20 mg of NOV. The concentration of NOV was determined with an extinction coefficient of 4.15 mg^{-1} ml cm^{-1} at 260 nm, an A_{260}/A_{280} ratio of 1.64 or greater was expected.

Crystallization

Nodamura virus readily crystallized in moderate ionic strength solutions. The pellet in the final step of the purification often shattered to form small crystallites. Crystals were grown by vapor diffusion using the sitting-drop method (McPherson, 1982). In the typical crystallization, 10–15 μl of 7 mg ml^{-1} NOV in phosphate buffer was mixed with one volume of citrate buffer and equilibrated *versus* 20 ml of citrate buffer (0.24–0.28 *M* sodium citrate, pH adjusted to 6.0 with acetic acid, or 0.24 *M* potassium citrate pH 6.0, both with 0.1% β-octyl glucopyranoside). Crystals with a plate-like morphology usually appeared within a week. Crystals grown in the absence of detergent had one lattice constant of ~1100 Å. Two or more rounds of macro-seeding were required to consistently obtain diffraction quality crystals (the largest crystals were about 0.9 × 0.5 × 0.3 mm). Crystals usually diffracted to greater than 2.9 Å resolution.

Data collection and processing

Diffraction patterns were collected on 11 × 11 cm film by oscillation photography at the F-1 station of the Cornell High Energy Synchrotron Source (CHESS) using a 0.3 mm collimator. The oscillation angle was 0.3°. The X-ray wavelength was 0.91 Å. A crystal-to-film distance of 210 mm, resulting in the collection of data to only 3.3 Å, minimized overlaps of reflections.

Films were digitized on an Optronics drum scanner at 50 μm raster step. Initially, unit-cell dimensions and orientation of the randomly set crystals were determined with the auto-indexing program of Kim (1989). Later, crystal orientation was determined with the programs of Kim (1989) or Kabsch (1988). Crystal setting was refined and reflections integrated with the film processing program of Rossmann (1979).

Data

The data set used for the analysis described in this report was comprised of 101 films from 16 crystals. Typically 30 000 whole and partial reflections (Table 1) were predicted for each film. Films had up to 20 000 reflections with $I/\sigma(I)$ greater than 2. A total of 2.2 million predicted observations yielded 910 000 unique reflections with $I/\sigma(I)$ greater than 3. The data were scaled together and post-refined (Rossmann, Leslie, Abdel-Meguid & Tsukihara, 1979) to an R_{merge} of 13.8%. R_{merge} is defined as

$$R_{merge} = \left[\left(\sum_h \sum_i |I_h - I_{hi}|\right)/\left(\sum_h I_{hi}\right)\right] \times 100\%$$

where I_{hi} is the intensity of the ith observation of a reflection h with a mean intensity of I_h.

Results and discussion

Unit cell and packing

Unit-cell dimensions were initially determined by auto-indexing a group of 0.3° oscillation films. The films indexed as monoclinic with dimensions close to the post-refined values of $a = 562.9$, $b = 354.4$, $c =$

Table 1. *Independent reflections in the data set for the monoclinic NOV crystals*

Shell (Å)	Reflections in shell	Total No. of reflections	Theoretical No. in shell	Theoretical total	% in shell	% total
25–20	3042	3042	7303	7303	42	42
20–13	13421	16463	39526	46829	34	35
13–9	40468	56931	109728	156557	37	36
9–7	65176	122107	184807	341364	35	36
7–6	66594	188701	223215	564579	30	33
6–5.4	67422	256123	188035	752164	36	34
5.4–4.8	106657	362780	322227	1074841	33	34
4.8–4.3	137305	500085	423227	1498068	32	33
4.3 3.9	146637	646722	512445	2010513	29	32
3.9–3.6	135703	782425	547757	2558270	25	31
3.6 3.3	127888	910313	765356	3323626	17	28

613.4 Å, $\beta = 110.9°$. Pseudo-$C2$ symmetry was seen at low resolution in NOV data as systematically weak $h + k$ odd reflections (Fig. 1). A nominal difference is observed between even and odd $h + l$ and $k + l$ reflections, suggesting some degree of pseudo-centering in the A and B faces. A similar case of pseudo-symmetry was observed in the case of Coxsackie virus $B3$ crystals (presented by Bibler & Rossmann at the NATO Advanced Study Institute and EEC Course on the Regulation of Gene Expression by Animal Viruses, 1992).

The V_m was 3.25 Å^3 Da^{-1} for four 8.8×10^6 Da virus particles per unit cell, two crystallographically independent particles per asymmetric unit. Though this V_m is large for a protein it is not atypical for virus crystals. For instance, southern bean mosaic virus in its $R32$ setting had $V_m = 3.6$ Å^3 Da^{-1} for one virus per unit cell; in its orthorhombic $C222_1$ setting $V_m = 3.5$ Å^3 Da^{-1} for four viruses per unit cell (Akimoto, Wagner, Johnson & Rossmann, 1975).

To account for all four particles in the NOV unit cell, a rhombohedral packing arrangement was hypothesized with the virus at special positions in a $C2$ unit cell (Fig. 2 and Table 2). The pseudo-$R32$ packing was the result of a search for positions in a C-centered monoclinic cell consistent with a virus radius of > 320 Å, an isometric environment for each particle in the unit cell, and the icosahedral symmetry of the particle.

The following discussion refers to the hypothetical non-primitive monoclinic unit cell. The special position of $xyz = 00\frac{1}{4}$ created face centering in the monoclinic setting (Fig. 2 and Table 2). The angle between virus particles forming the vertices of the rhombohedral cell was either 64.4 or 115.6°, approximately the angle between adjacent icosahedral fivefold axes. This suggests that the icosahedral fivefold axes were involved in crystal packing and constrained the virus particle orientation. The closest inter-particle distance was 332.6 Å. These dimensions define the $R32$ unit cell as $a = b = c = 332.6$ Å, $\alpha = \beta = \gamma = 64.4°$. When the particles were arranged so that the closest contact was along a fivefold axis, a pair of orthogonal icosahedral twofold axes were parallel to the monoclinic twofold axis, b, and to the a axis.

The relationship between the $C2$ and $R32$ reciprocal space lattices is described by the following transformation matrices (see *International Tables for Crystallography*, Vol. A, §5.2)

$$\begin{pmatrix} h \\ k \\ l \end{pmatrix}_{R32} = \begin{pmatrix} \frac{1}{2} & \frac{1}{2} & \frac{1}{2} \\ -\frac{1}{2} & \frac{1}{2} & 0 \\ 0 & 0 & \frac{1}{2} \end{pmatrix} \begin{pmatrix} h \\ k \\ l \end{pmatrix}_{C2} \qquad (1a)$$

$$\begin{pmatrix} h \\ k \\ l \end{pmatrix}_{C2} = \begin{pmatrix} 1 & -1 & -1 \\ 1 & 1 & -1 \\ 0 & 0 & 2 \end{pmatrix} \begin{pmatrix} h \\ k \\ l \end{pmatrix}_{R32} . \qquad (1b)$$

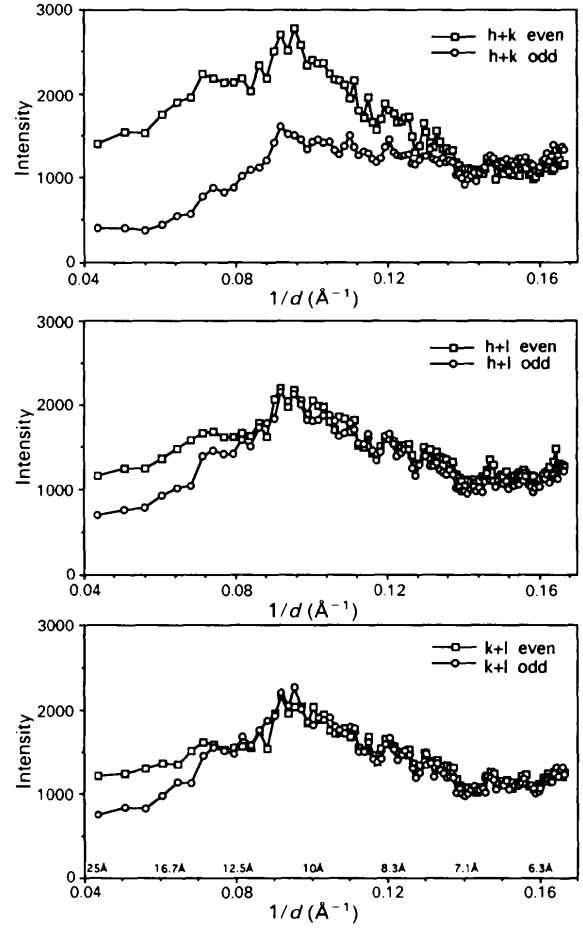

Fig. 1. The average intensities of $h + k$ odd reflections are notably weaker than $h + k$ even reflections, indicating pseudo-C centering. Systematic weakness in the $h + l$ face and the $k + l$ face are also evident, though the difference between odd and even pairs of reflections was not as strong. In these plots, all data between 25 and 6 Å are separated into odd or even files of reflections which are then divided into 100 equal volume resolution bins. There is an average of 900 reflections per bin.

In the transformation from the $C2$ to the $R32$ lattice (1*a*), only even $h + k$, $h + l$ and $k + l$ Miller indices in the monoclinic setting will yield integer $R32$ lattice points. By the same logic, the transformation matrix from the $R32$ to the $C2$ lattice (1*b*) only yields lattice points that have even indices. These conditions for reflections are the extinctions associated with a face-centered lattice in a monoclinic setting. Because the NOV crystal has $R32$ pseudo-symmetry, instead of systematic absences we observe systematic weaknesses in Fig. 1.

Examination of the unit-cell dimensions indicated there is a geometric deviation from the ideal packing diagram (Fig. 2). Considering the $C2$ positions for the virions, the $R32$ *a* and *b* axes are 332.6 Å but the *c* axis is 334.2 Å. Thus, the $R32$ and/or the $C2$ symmetry must be broken.

(There was an alternative arrangement for an $R32$ unit cell with icosahedra at special positions. The icosahedra were rotated 60° about their threefold axis, parallel to the body diagonal, from the orientation shown in Fig. 2. The role of the fivefold axes, suggested by the 64.4° inter-particle angle in the case of NOV, did not play an obvious role in packing or inter-particle contacts in this $R32$ setting. This alternative $R32$ setting was eliminated from further consideration by rotation function analysis.)

Rotation function results

Icosahedral viruses have 532 point-group symmetry resulting in up to 60-fold non-crystallographic symmetry per virus. Non-crystallographic symmetry operators can be identified with a rotation function search (Rossman & Blow, 1962). The packing diagram described previously defines position and orientation of the virus. A rotation function was used to determine the orientation of the virus, testing the pseudo-$R32$ packing.

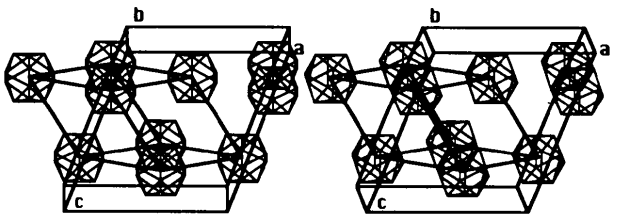

Fig. 2. Idealized packing diagram. The virus particles are positioned in the monoclinic cell by assuming the pseudo-$C2$ symmetry. Note that an icosahedral twofold axis is parallel to the monoclinic **b** axis. An icosahedral threefold axis is parallel to the monoclinic 101 axis and defines the body diagonal of the rhombohedral unit cell. Unit-cell dimensions for the monoclinic cell are $a = 562.9$, $b = 354.4$, $c = 613.4$ Å, $\beta = 110.9°$. The rhombohedral dimensions are $a = 332.6$ Å, $\alpha = 64.4°$. The diameter of the icosahedra in this illustration are reduced, compared to the virus diameter, for clarity.

Table 2. *Virus positions located in a pseudo-C2 pseudo-R32 unit cell*

$C2$ symmetry	$C2$ special positions								
(*A*) x, y, z	0	0	$\frac{1}{4}$	$\frac{1}{4}$	0	0	$\frac{1}{4}$	0	$\frac{1}{4}$
(*B*) $-x, \frac{1}{2}+y, -z$	0	$\frac{1}{2}$	$\frac{3}{4}$	$\frac{1}{4}$	$\frac{1}{2}$	0	$\frac{3}{4}$	$\frac{1}{2}$	$\frac{1}{4}$
(*a*) $\frac{1}{2}+x, \frac{1}{2}+y, z$	$\frac{1}{2}$	$\frac{1}{2}$	$\frac{3}{4}$	$\frac{3}{4}$	$\frac{1}{2}$	$\frac{1}{2}$	$\frac{3}{4}$	$\frac{1}{2}$	$\frac{3}{4}$
(*b*) $\frac{1}{2}-x, y, -z$	$\frac{1}{2}$	0	$\frac{3}{4}$	$\frac{3}{4}$	0	$\frac{1}{2}$	$\frac{3}{4}$	0	$\frac{3}{4}$

Notes: In the given unit cell the special positions are consistent with the transformation from a monoclinic to a rhombohedral setting described by equations (1*a*) and (1*b*). The alternative special positions result in different primitive monclinic space groups when higher symmetry is broken, as shown in Fig. 7. The positions given in columns 2 and 3 form distinct $P2_1$ unit cells (Figs. 7*b* and 7*c*, respectively) and those in column 4 form a $P2$ unit cell (Fig. 7*a*).

Rotation function results are described by a polar coordinate convention where the crystal *b* axis is coincident with the orthogonal reference frame *y* axis and *c* is coincident with *z* (Fig. 3*a*; Rossmann & Blow, 1962). In a standard icosahedral setting three mutually perpendicular icosahedral twofold axes are coincident with the reference coordinate system axes (Fig. 4*a*).

The orientation of an icosahedron in an $R32$ unit cell, in the $C2$ setting is defined in Figs. 3(*b*) and 4(*b*).

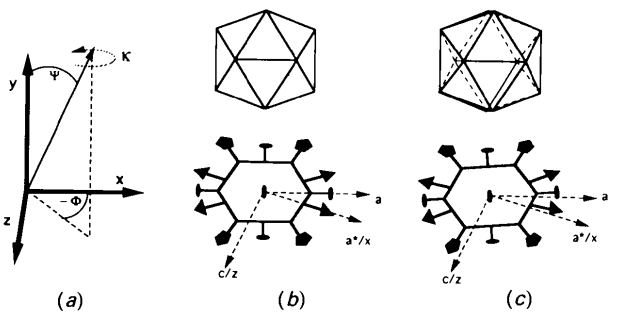

Fig. 3. The rotation function polar coordinate system. An icosahedron and an equatorial projection of the icosahedral symmetry operators are projected onto the monoclinic unit-cell axes and the rotation coordinate system *xz* plane in (*b*) and (*c*). (*a*) The polar coordinate reference frame for the rotation functions is described in detail below. An icosahedral twofold is coincident with the reference *y* axis. (*b*) The setting for a virus in a rhombohedral unit cell with a monoclinic setting. The icosahedral threefold axis is 20.9° from the monoclinic *a* axis and is coincident with the rhombohedral body diagonal, which is also the monoclinic a^* axis. (*c*) The locked rotation function result of $\kappa = 23°$ suggests that the standard icosahedron is rotated 23° from a^*, the icosahedral threefold is not aligned with the pseudo-rhombohedral body diagonal. For clarity the angle between the threefold and a^* in this figure is 5° instead of 2.1°. In this convention the *b* axis of the unit cell is coincident with the *y* axis of the reference coordinate system. The unit-cell *c* axis lies in the *yz* plane, for a monoclinic unit cell *c* is coincident with *z*. The *a* axis of the unit cell is not restricted, but, to form an orthogonal reference coordinate system, the *x* axis will be coincident with a^*. The angle between the axis of rotation and the reference *y* axis is ψ and the projection of the rotation axis into the *xz* plane is φ. The rotation about this axis is κ.

An icosahedral twofold is coincident with the reference y axis and a threefold axis, perpendicular to the twofold, should lie on the 101 axis. Fig. 3 shows a projection of icosahedral symmetry elements into the xz plane of the reference frame. A more detailed description of the arrangement of icosahedral symmetry operators is seen in the stereo net in Fig. 4. The equator of the icosahedral virus, around the twofold axis in the $R32$ setting ($\psi = 90°$, $\varphi =$ 180–360°), has a threefold axis lying along the reference x axis (Fig. 3*b*) 20.9° from the a axis of the monoclinic unit cell.

A locked rotation function makes use of all icosahedral symmetry operators at each point in the search, thus it is especially useful in an incomplete data set (Tong & Rossmann, 1990). Since the standard orientation of icosahedral symmetry operators has a twofold axis coincident with the reference frame y axis (Fig. 5*a*), as does a virus in the $R32$ setting (Fig. 5*b*), a locked rotation function can be reduced to a one-dimensional search in κ, with φ and ψ set to 0°. Data in two resolution shells, 11.0–8.5 and 3.9–3.7 Å, which were 36 and 25% complete, respectively, were used. Self and locked rotation functions reported here were computed with the high-resolution shell containing 80 000 reflections with 1200 large terms, using the program *GLRF* (Tong & Rossmann, 1990). Large terms are structure factors that are greater than 3.5 times the average of all structure factors. Similar results were found with

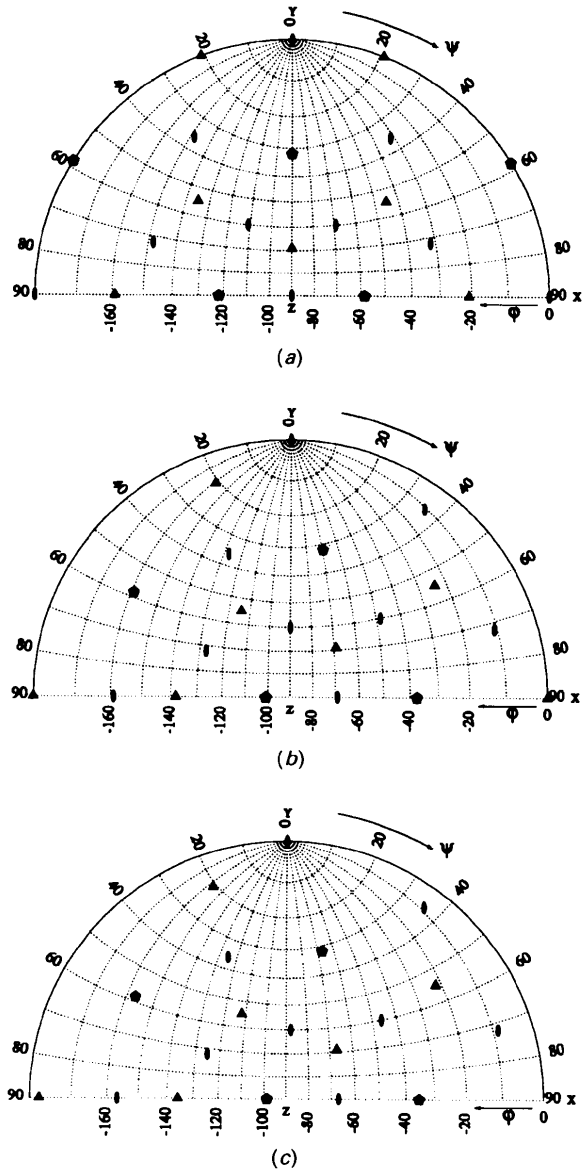

Fig. 4. Stereographic projections of icosahedral symmetry operators showing (*a*) a standard icosahedral orientation, (*b*) an icosahedron oriented in an $R32$ setting, and (*c*) the orientation of NOV. In the rhombohedral setting note that at $\psi = 90°$ a threefold axis lies on $\varphi = 0$ and 180°. The standard icosahedral setting is defined as having three orthogonal twofold axes at φ–ψ values of 0 and 0, 0 and 90, and 90 and 90°, respectively. Only half of a hemisphere is shown because, in all three cases, two mutually perpendicular icosahedral twofolds at $\psi = 90°$ generate a mirror plane.

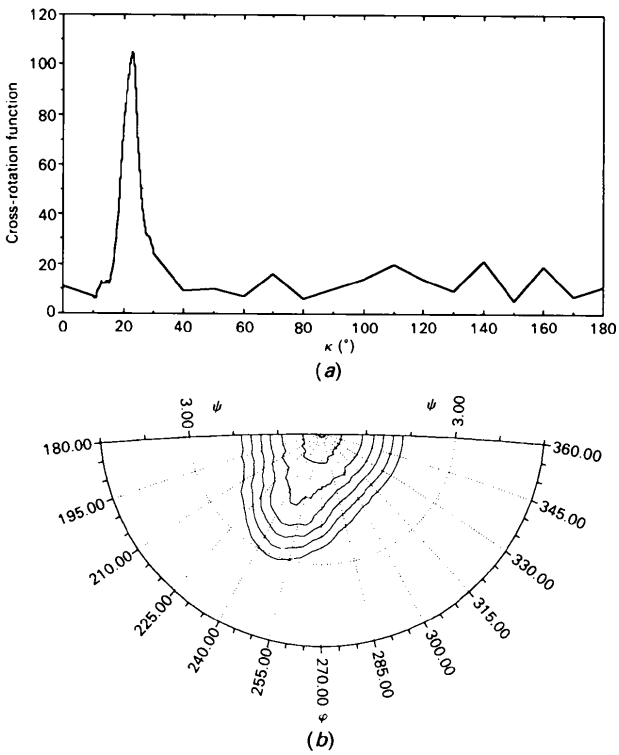

Fig. 5. Locked self-rotation function results. (*a*) A single peak at $\kappa = 23°$ is found for φ and ψ equal to 0°. (*b*) A general search in all three polar angles yielded a similar result. 86 000 reflections and 1100 large terms between 3.9 and 3.7 Å are used in this calculation. High-resolution data were used in an effort to identify two orientations for the virus.

the low-resolution shell. The radius of integration is 150 Å, although results are nearly identical when radii of 140 or 120 Å were used. Patterson origins were subtracted from all of the rotation functions described here.

In the one-dimensional locked rotation function a single peak ($\sigma = 7.5°$) was found at $\kappa = 23.0°$ (Fig. 5*a*). The standard icosahedron must be rotated 23° about the rotation coordinate system y axis, 2.1° from the rhombohedral setting, to align with the NOV icosahedral symmetry elements in the monoclinic unit cell. This rotation is illustrated as an equatorial projection of icosahedral symmetry operators in Fig. 3(*c*) and as a stereographic net in Fig. 4(*c*). The rotation of the icosahedral threefold axis from the body diagonal breaks the rhombohedral symmetry but does not, by itself, break the pseudo-$C2$ symmetry. A three-dimensional locked rotation function revealed a single peak, which indicates that the two viruses have identical or nearly identical orientations. The single peak centered at $\varphi = \psi = 0°$, $\kappa = 23°$ is asymmetric (Fig. 5*b*), which may indicate the presence of several unresolved peaks, but this cannot be interpreted with confidence.

A cross rotation function *versus* FHV (Fig. 6) tests the locked rotation function result and minimizes artifacts arising as a result of the paucity of data. A complete data set, including observed and calculated structure factors is available for FHV (Fisher, personal communication). The FHV forms the stationary lattice and large terms from NOV are rotated against it. The cross rotation function, calculated using the program *GLRF* (Tong & Rossmann, 1990), employed data between 11.0–8.5 Å. FHV crystallized in a rhombohedral ($R3$) unit cell, where the virus is rotated 23° about the rhombohedral threefold axis from the alternative $R32$ setting, described previously. The expected cross rotation result is 60 + 23 = 83°. By prerotating the FHV and the NOV icosahedral threefold axes onto the reference frame y axis, this rotation function also reduces to a one-dimensional search in κ. In this calculation, we are looking for agreement with the results of the locked rotation function. The orientation of the single 11σ peak at 83.5° is 0.5° from the expected result, corresponding to a positional error $\simeq 1.3$ Å at the surface of a 310 Å diameter particle. In the higher resolution range the background noise was much greater.

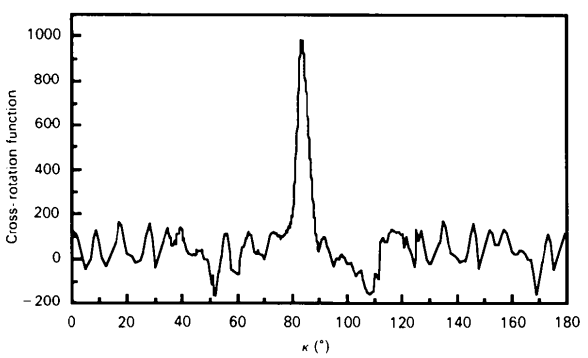

Fig. 6. Cross rotation function *versus* FHV. The FHV and NOV icosahedral threefold axes were aligned with the reference coordinate system y axis. 15 000 reflections from FHV, all observed and calculated structure factors between 11.0 and 8.5 Å, were compared to 770 large terms (3.5 times average intensity) from NOV.

Patterson function results

Examination of the particle positions of a rhombohedral unit cell in the monoclinic setting reveals unusual symmetry. In addition to the $C2$ symmetry, an array of symmetry operators are generated along $a = \frac{1}{4}$ and $\frac{3}{4}$ (Fig. 7*a*). These are an effect of the special positions of the viruses in the monoclinic cell. The twofold and two 2_1 axes are related by a change of origin in the $C2$ unit cell. When $C2$ symmetry breaks down, the additional symmetry operators cause an ambiguity in the choice of origin (Figs. 7*b* and 7*c*). In the $P2_1$ unit cell, one 2_1 axis is defined by crystal symmetry, the other axis is a result of a pseudo-symmetric, non-crystallographic relationship between the two virus particles in the asymmetric unit. Thus, the two possible $P2_1$ unit cells have different non-equivalent asymmetric units. In the case of Fig. 7(*b*) an asymmetric unit of particles $A + a$ are related to $B + b$ to by a 2_1 axis, in Fig. 7(*b*), particles $A + B$ are related to $a + b$.

In the $C2$ cell, the special positions of virus particles yield a distinctive, face-centered Patterson map. Patterson peaks are possible only because viral and crystallographic twofold axes are parallel. Because application of a twofold symmetry operation to a twofold symmetry operation results in an identity operation, all particles are in the same orientation and yield clear Patterson peaks. The Patterson vectors resulting from the array of symmetry operations only have **u**, **v** and **w** values of 0 or a half (Fig. 7*a*). The face-centered Patterson map (Fig. 8) confirms the hypothesized packing diagram.

The Patterson map gives the opportunity to positively identify where the $C2$ symmetry breaks down because of translation of the virus particles. Even at low resolution, it is clear from the splitting of the expected peaks that the viruses are not at the $R32$ special positions (Fig. 8). Though $C2$ symmetry breaks down at low resolution, there still remains a question as to which of the three possible twofold axes is crystallographic and which are pseudo-twofolds. Systematic absences for $0k0$ odd reflections suggest that the monoclinic symmetry is $P2_1$ due to one of two distinct 2_1 screw axes. Ambiguities in the Patterson map, broad peaks and Fourier ripple,

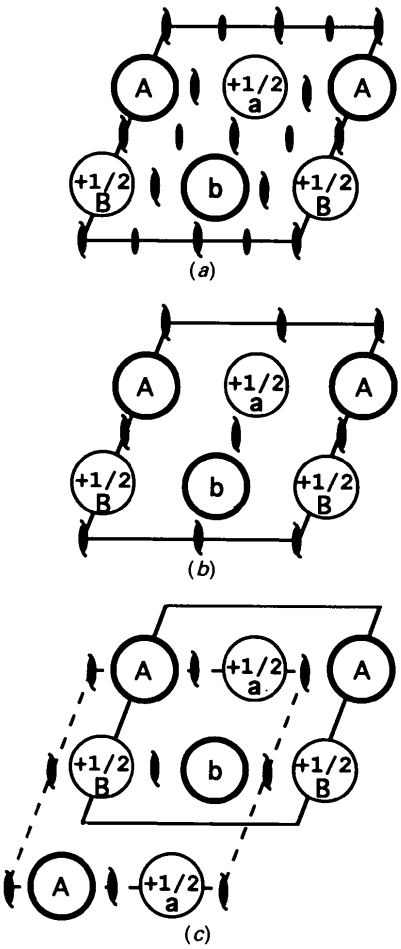

Fig. 7. (*a*) Symmetry operators in an *R*32 cell in the *C*2 setting. Each virus sits on a twofold axis. Note the two distinct classes of 2_1 screw axes; one set of screw axes is generated by the special positions of the particles. There is no distinction between twofold axes. (*b*) A $P2_1$ unit cell where crystal symmetry relates *A* to *B* and *a* to *b*. (*c*) The alternative $P2_1$ setting where *A* is crystallographically related to *a*, and *B* to *b*.

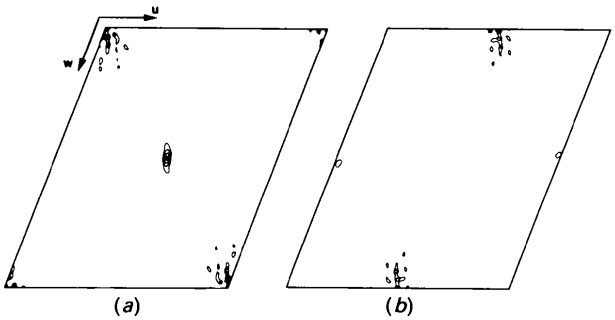

Fig. 8. A Patterson map of NOV computed with all data from 20–10 Å. (*a*) Harker section $v = 0$. Even at low resolution, the peak centered at $\frac{1}{2}0\frac{1}{2}$ has two maxima. (*b*) Harker section at $v = \frac{1}{2}$. The peaks predicted at $\frac{1}{2}\frac{1}{2}0$ and $0\frac{1}{2}\frac{1}{2}$ are seen, close to those positions for the *C*2 cell. The peak near $0\frac{1}{2}\frac{1}{2}$ is notably displaced from $\mathbf{u} = 0$. Only positive density is shown; contours are at 6σ.

partly as a result of the paucity of data, prevent determination of the virus position and the true symmetry axis.

Concluding remarks

Nodamuravirus crystallizes in a monoclinic space group. We have taken advantage of the pseudo-*C*2/*R*32 symmetry to develop a packing model. Analysis of a limited sample of crystallographic data by rotation function and native Patterson maps, with respect to the packing model, has shown where higher symmetry has broken down both rotationally and translationally. The *R*32 symmetry was broken by a rotation of the icosahedral threefold axis from the body diagonal of the *R*32 cell. Broad rotation function peaks suggest that the viruses in the asymmetric unit may be in slightly different orientations. The *C*2 symmetry may also be broken translationally.

As more data are processed, virus orientation and position will be refined before proceeding with determination of the 3.3 Å resolution structure of NOV by molecular replacement with an FHV poly-alanine model.

We would like to thank Liang Tong for helpful discussions on pseudo-symmetry. AZ and JB were partially supported by an NIH Biophysics training grant (GM08296). This work was funded by an NIH grant (GM34220) to JEJ; an NIH grant (AI11219), an NSF grant (MCB9102855) and funds from the Sterling–Winthrop Pharmaceutical Research Division to MGR; and a Lucille P. Markey Foundation grant to support structural studies. We also acknowledge the Cornell High Energy Synchrotron Source (CHESS) data collection facility.

References

AKIMOTO, T., WAGNER, M. A., JOHNSON, J. E. & ROSSMANN, M. G. (1975). *J. Ultrastruct. Res.* **53**, 306–318.

DASGUPTA, R. & SGRO, J.-Y. (1989). *Nucleic Acids Res.* **12**, 7525–7526.

DAVIS, P. B. & PEARSON, C. K. (1978). *Anal Biochem.* **91**, 343–349.

FISHER, A. J. & JOHNSON, J. E. (1993). *Nature (London)*, **361**, 176–179.

FISHER, A. J., MCKINNEY, B. R., WERY, J.-P. & JOHNSON, J. E. (1992). *Acta Cryst.* B**48**, 515–520.

GALLAGHER, T. M. & RUECKERT, R. R. (1988). *J. Virol.* **62**, 3399–3406.

HENDRY, D. (1991). *Viruses of Inverterates*, edited by E. KURSTAK, pp. 227–276. New York: Marcel Dekker.

HOSUR, M. V., SCHMIDT, T., TUCKER, R. C., JOHNSON, J. E., GALLAGHER, T. M., SELLING, B. H. & RUECKERT, R. R. (1987). *Proteins Struct. Funct. Genet.* **2**, 167–176.

KABSCH, W. (1988). *J. Appl. Cryst.* **21**, 67–71.

KAESBERG, P. (1987). *Molecular Biology of Positive Strand RNA Viruses*, edited by D. J. ROWLANDS, M. A. MAYO, B. W. J. MAHY, pp. 207–218. London: Academic Press.

KAESBERG, P., DASGUPTA, R., SGRO, J.-Y., WERY, J.-P., SELLING, B. H., HOSUR, M. V. & JOHNSON, J. E. (1990). *J. Mol. Biol.* **214**, 423–435.

KIM, S. (1989). *J. Appl. Cryst.* **22**, 53–60.

MCPHERSON, A. (1982). *Preparation and Analysis of Protein Crystals*. New York: John Wiley.

NEWMAN, J. F. E. & BROWN, F. (1977). *J. Gen. Virol.* **38**, 83–95.

NEWMAN, J. F. E., MATTHEWS, T., OMILIANOWSKI, D. R., SALERNO, T., KAESBERG, P. & RUECKERT, R. (1978). *J. Virol.* **25**, 78–85.

ROSSMANN, M. G. (1979). *J. Appl. Cryst.* **12**, 225–238.

ROSSMANN, M. G. & BLOW, D. M. (1962). *Acta Cryst.* **15**, 24–31.

ROSSMANN, M. G., LESLIE, A. G. W., ABDEL-MEGUID, S. S. & TSUKIHARA, T. (1979). *J. Appl. Cryst.* **12**, 570–581.

SCHNEEMAN, A., ZHONG, W., GALLAGHER, T. M. & RUECKERT, R. R. (1992). *J. Virol.* **66**, 6728–6734.

SELLING, B. (1986). PhD dissertation, Univ. of Wisconsin, USA.

TONG, L. & ROSSMANN, M. G. (1990). *Acta Cryst.* A**46**, 783–792.

TUCKER, R. C. (1990). MS dissertation, Purdue Univ. USA.

ZLOTNICK, A., REDDY, V., SCHNEEMANN, A., DASGUPTA, R., RUECKERT, R. & JOHNSON, J. E. (1993). In preparation.